Tree Physiology 42, 208–224
https://doi.org/10.1093/treephys/tpab006

Research paper

Photoprotective compounds as early markers to predict holm oak crown defoliation in declining Mediterranean savannahs

Manuel Encinas-Valero[1,†], Raquel Esteban[2,6†], Ana-Maria Hereş[1,3], José María Becerril[2], José Ignacio García-Plazaola[2], Unai Artexe[2], María Vivas[4], Alejandro Solla[4], Gerardo Moreno[4] and Jorge Curiel Yuste[1,5]

[1]BC3-Basque Centre for Climate Change, Scientific Campus of the University of the Basque Country, 48940 Leioa, Bizkaia, Spain; [2]Department of Plant Biology and Ecology, University of Basque Country (UPV/EHU), Barrio Sarriena s/n, 48940 Leioa, Bizkaia, Spain; [3]Department of Forest Sciences, Transilvania University of Braşov, Sirul Beethoven-1, 500123 Braşov, Romania; [4]Faculty of Forestry, Institute for Dehesa Research (INDEHESA), University of Extremadura, Avenida Virgen del Puerto 2, 10600 Plasencia, Spain; [5]IKERBASQUE, Basque Foundation for SciencePlaza Euskadi 548009 Bilbao, Bizkaia, Spain; [6]Corresponding author (raquel.esteban@ehu.eus)

Received September 25, 2020; accepted January 4, 2021; handling Editor ülo Niinemets

Dehesas, human-shaped savannah-like ecosystems, where the overstorey is mainly dominated by the evergreen holm oak (*Quercus ilex* L. subsp. *ballota* (Desf.) Samp.), are classified as a global conservation priority. Despite being *Q. ilex* a species adapted to the harsh Mediterranean environmental conditions, recent decades have witnessed worrisome trends of climate-change-induced holm oak mortality. Holm oak decline is evidenced by tree vigour loss, gradual defoliation and ultimately, death. However, before losing leaves, trees undergo leaf-level physiological adjustments in response to stress that may represent a promising field to develop biochemical early markers of holm oak decline. This study explored holm oak photoprotective responses (pigments, tocopherols and photosynthetic performance) in 144 mature holm oak trees with different health statuses (i.e., crown defoliation percentages) from healthy to first-stage declining individuals. Our results indicate differential photochemical performance and photoprotective compounds concentration depending on the trees' health status. Declining trees showed higher energy dissipation yield, lower photochemical efficiency and enhanced photoprotective compounds. In the case of total violaxanthin cycle pigments (VAZ) and tocopherols, shifts in leaf contents were significant at very early stages of crown defoliation, even before visual symptoms of decline were evident, supporting the value of these biochemical compounds as early stress markers. Linear mixed-effects models results showed an acute response, both in the photosynthesis performance index and in the concentration of foliar tocopherols, during the onset of tree decline, whereas VAZ showed a more gradual response along the defoliation gradient of the crown. These results collectively demonstrate that once a certain threshold of leaf physiological damage is surpassed, that leaf cannot counteract oxidative stress and progressive loss of leaves occurs. Therefore, the use of both photosynthesis performance indexes and the leaf tocopherols concentration as early diagnostic tools might predict declining trends, facilitating the implementation of preventive measures to counteract crown defoliation.

Keywords: defoliation, drought-induced dieback, holm oak, performance index, stress markers, tocopherol, xanthophylls.

†These authors contributed equally to this work.

Introduction

An increasing number of reports highlight that climate-change-induced tree decline and mortality events represent a worldwide phenomenon of global importance (Allen et al. 2010, Hartmann et al. 2018). Potential consequences of tree decline and subsequent mortality on ecosystem functioning (Curiel Yuste et al. 2019, Rodríguez et al. 2019, García-Angulo et al. 2020), land–atmosphere interactions (Anderegg et al. 2013, Bonan 2016) and ecosystem services (Breshears et al. 2011, Xiong et al. 2011) are large and difficult to disentangle. Therefore, it is of utmost importance to identify the early events and physiological causes of tree decline, aiming to improve and develop predictive tools for early diagnosis.

The Mediterranean basin, a biodiversity hotspot of global conservation priority (Bellard et al. 2014, Matesanz and Valladares 2014), is one of the regions of the world where the number of climate-change-induced tree decline and mortality events has increased the most during the last decades (Carnicer et al. 2011, Martínez-Vilalta et al. 2012, Natalini et al. 2016, Gazol et al. 2020). Within the Mediterranean region, the dehesas (Spain) or montados (Portugal), which are human-shaped savannah-like ecosystems, are among the most threatened ecosystems (Pulido et al. 2001, Herguido-Sevillano et al. 2017). The causes that underlie the phenomenon of tree decline are complex, varying from purely climatic ones (Natalini et al. 2016, Hereş et al. 2018, García-Angulo et al. 2020) to the occurrence of soil-borne pathogen outbreaks, mainly of *Phytophthora* spp. (Brasier 1996, Solla et al. 2009, Martín-García et al. 2015). However, in most cases, the interactions of different factors explain better the declining trend than a single stressor (Thomas 2008, de Sampaio e Paiva Camilo-Alves et al. 2013, Gómez et al. 2019)

The dominant tree species in dehesas ecosystems are evergreen broadleaf species from the *Quercus* genus, especially the holm oak (*Quercus ilex* L. subsp. *ballota* (Desf.) Samp.) and the cork oak (*Quercus suber* L.) (Pulido et al. 2001, Moreno and Pulido 2009). Holm oak is a tree species that is well-adapted to the harsh conditions of the Mediterranean continental climate, and it thrives well in hot and dry summers and cold winters (Canadell et al. 1992, Ramírez-Valiente et al. 2020). During the last decades, holm oak has started to show a worrisome symptomatic declining trend (i.e., root rot, carbon starvation, hydraulic failure, leaves wilting, stem mortality, defoliation reduced carbon gain potential) followed by high mortality rates (Pollastrini et al. 2019, Ogaya et al. 2020). The oomycete *Phytophthora cinnamomi* Rands has been considered as the main factor responsible for the loss of its vigour, decline and mortality in Southern Europe (Brasier 1996, Sánchez et al. 2002) and especially in the western part of the Iberian Peninsula. Pathogen-induced symptoms resemble those of drought (de Sampaio e Paiva Camilo-Alves et al. 2013) and occur primarily due to a loss of fine roots and ectomycorrhizal root tips (Corcobado et al. 2014). The immediate consequence is a loss in tree water uptake ability (hydraulic failure) in combination with a reduction in non-structural carbohydrates that lead to carbon starvation (Ogaya et al. 2020), which results in a rapid wilting of leaves of one part of the canopy and/or in a gradual loss of foliage (crown defoliation), followed by tree death after one or two growing seasons (Brasier 1996, Gallego et al. 1999, Corcobado et al. 2013). Besides, *Q. ilex* species showed higher stem mortality than other Mediterranean species (Ogaya et al. 2020), which leads to ecosystem composition alteration. Therefore, crown defoliation in holm oaks, which is the consequence of the physiological loss of tree vigour, is generally attributed to the activity of this soil-borne pathogen (i.e., *Phytophthora* spp.), drought stress or, more realistically, to the interaction of both factors (Gómez-Aparicio et al. 2012, Poyatos et al. 2013, Esteban et al. 2014).

Before crown defoliation occurs, a set of fine-tuning biochemical adjustments are triggered at leaf level (Fernández-Marín et al. 2017), reflecting profound modifications of the photosynthetic apparatus (Esteban et al. 2015*a*). These adjustments involve a variety of photoprotective mechanisms, mainly regulated by specialized metabolites, which may include: pigment concentration adjustments, the activation of xanthophyll cycles (both violaxanthin, VAZ and lutein epoxide-lutein, LxL; Esteban and García-Plazaola 2014) and the antioxidant network (Fernández-Marín et al. 2017), such as the tocopherols that act as scavengers of reactive oxygen species (Munné-Bosch 2005, Nogués et al. 2014). Enhancement of these metabolites, triggered under moderate stress, may be good predictors of plant fitness (Fernández-Marín et al. 2017). For this reason, metabolites are widely employed as early stress markers to evaluate and predict plant physiological status (García-Plazaola and Becerril 2001, Tausz et al. 2004, Munné-Bosch and Lalueza 2007, Esteban et al. 2009*a*, Fenollosa and Munné-Bosch 2018). In the case of *Quercus* spp., the photosynthetic efficiency (Bussotti 2004, Holland et al. 2014) and the pigment (i.e., chlorophylls and carotenoids; Nogués et al. 2014, Ramírez-Valiente et al. 2015) or tocopherols content (Camarero et al. 2012) have been employed to evaluate photoprotective responses under a wide variety of environmental conditions. However, unlike the huge body of knowledge currently available on early markers (Bussotti 2004, Camarero et al. 2012, Holland et al. 2014, Nogués et al. 2014, Ramírez-Valiente et al. 2015), their use as a crown defoliation warning indicator under Mediterranean forest decline scenarios has been poorly studied (García-Plazaola and Becerril 2001).

As stated above, the functioning of the antioxidant and photoprotection mechanisms in holm oaks have been relatively well studied and described. This knowledge could therefore be used to develop biochemical markers of environmental stress in native holm oak trees, which would be of paramount importance for the early diagnosis of tree decline. Therefore, the

aims of the present study were (i) to identify plant performance markers that precede crown defoliation in holm oak trees with contrasting health status using chlorophyll *a* fluorescence induction, pigments and tocopherols, and (ii) to link these plant performance markers with tree defoliation, using a wide range of tree defoliation rates, to identify the physiological thresholds that may be used to predict tree decline. We hypothesized that before holm oak defoliation occurs, leaves undergo different physiological adjustments of their photoprotective compounds in line with the photochemical efficiency loss determined by an external mild perturbation. The stress markers proposed in this study may be considered as tools of high capacity for the diagnosis of early vigour losses at the plant and even ecosystem level. The results from this study therefore represent a data and theoretical baseline for the future applicability of tools able to predict in advance potential tree mortality events that may occur locally and even globally.

Materials and methods

Study sites

We considered eight holm oak dehesa sites, i.e., ecosystems characterized by a low density of trees (Pulido et al. 2001), as independent study sites. All these study sites were located in the central–western part of the Iberian Peninsula (Figure 1), at 430 ± 6 m above sea level. The plant community of these sites is defined as *Pyro bourgaeanae-Querceto rotundifoliae sigmentum* Rivas Mart. (Rivas-Martínez 1987). Here, scattered holm oak trees, with a low canopy cover (10–25%), grow in native permanent pastures dominated by annual species such as *Agrostis pourretii* Wild., *Xolantha guttata* (L.) Raf., *Plantago lagopus* L., *Vulpia myuros* (L.) C.C.Gmel., *Trifolium subterraneum* L., *Hordeum leporinum* Link, etc. Most of these dehesas have been traditionally used for livestock rearing and grazing, their average livestock being estimated at 0.4 units ha^{-1} $year^{-1}$. The pH of the soil varies from 4 to 7.7. The climate is Mediterranean, is characterized by hot and dry summers and mild winters. The mean monthly temperatures and rainfall in January and August 2019 were 6.96 °C, 29.88 mm, and 25 °C and 10.48 mm, respectively (CRU TS v.4; Harris et al. 2020, reference period 2019).

The selection of sites was performed based on a previous study (Corcobado et al. 2013), in which a combination of drought and *P. cinnamomi* were identified as the main tree decline causes. Specifically, for the final selection, we followed these criteria: (i) representative forests of the southwestern part of Spain, where dehesas abound; (ii) sites with trees at different stages of decline, from healthy to symptomatic (0 to 40% defoliation, respectively); (iii) sites were selected to define two distinctive situations, including plots with trees prominently healthy and plots in which healthy and affected trees coexisted; and (iv) sites with permission to conduct research and sampling (most of them are private properties).

Experimental design

Within each of the eight study sites (Figure 1), we identified and considered two areas of study, as in Corcobado-Sánchez (2013): one 'healthy' area, where the whole population of holm oak trees showed no evident signs of crown defoliation; and one 'declining' area, where both healthy and declining (i.e., defoliated) holm oak trees coexisted. From each of the healthy areas, we selected six healthy holm oak trees (hereinafter referred to as control trees). From each of the declining area, we selected 12 holm oak trees, as it follows: 6 healthy holm oak trees (asymptomatic with no signs of defoliation, hereinafter referred to as non-declining trees) and 6 holm oak trees with signs of defoliation and evidenced in higher crown transparency than asymptomatic trees and/or sparser foliage in small branches (Corcobado-Sánchez 2013) (hereinafter referred to as declining trees). Accordingly, within each study site, we selected 18 holm oak trees, with the total number of holm oak trees selected for the eight sites being 144 individuals. In each individual, crown-condition assessment, chlorophyll *a* fluorescence induction, and sampling for pigments and tocopherols determinations were performed during July 2019.

Crown assessment

In the field, we categorized individuals in healthy and declining holm oak trees based on their crown condition, as explained above. A posteriori, the quantitative crown condition was estimated using two independent methods: crown transparency (i.e., hereinafter referred to as crown defoliation), and relative irradiance at the floor level (i.e., the quantity of solar radiation below each selected holm oak tree). To estimate the crown defoliation, we took photographs of each selected holm oak tree (i.e., 144). These photographs were always taken south facing at a distance of 20 m from the holm oaks' trunks and at 1.65 m above ground using a digital camera in automatic mode (Canon Eos 1200D, Amstelveen, The Netherlands). Then, we developed a metric to quantify the crown condition processing images by estimating the total tree crown area and the defoliated areas within the crowns (i.e., branches with no leaves). Final crown defoliation was represented by the percentage of the total area occupied by the defoliated branches relative to the total crown area of the tree. This analysis was made with the Java-based image processing program ImageJ (1.52p; Ferreira and Rasband 2019, http://rsbweb.nih.gov/ij/). To estimate the relative irradiance at the floor level, we took hemispheric photographs below each selected holm oak tree. These photographs were always taken at a distance of 50 cm from the trunks of the trees and 2 m above ground using a Nikon Coolpix 4500 digital camera, mounted on a tripod and equipped with a Nikon Fisheye Converter. Photographs were then analyzed using the Gap Light Analyser (version 2.0; Frazer et al. 1999), which transforms the colours of the photographs into black and white to estimate their pixels and separated into the sky or non-sky

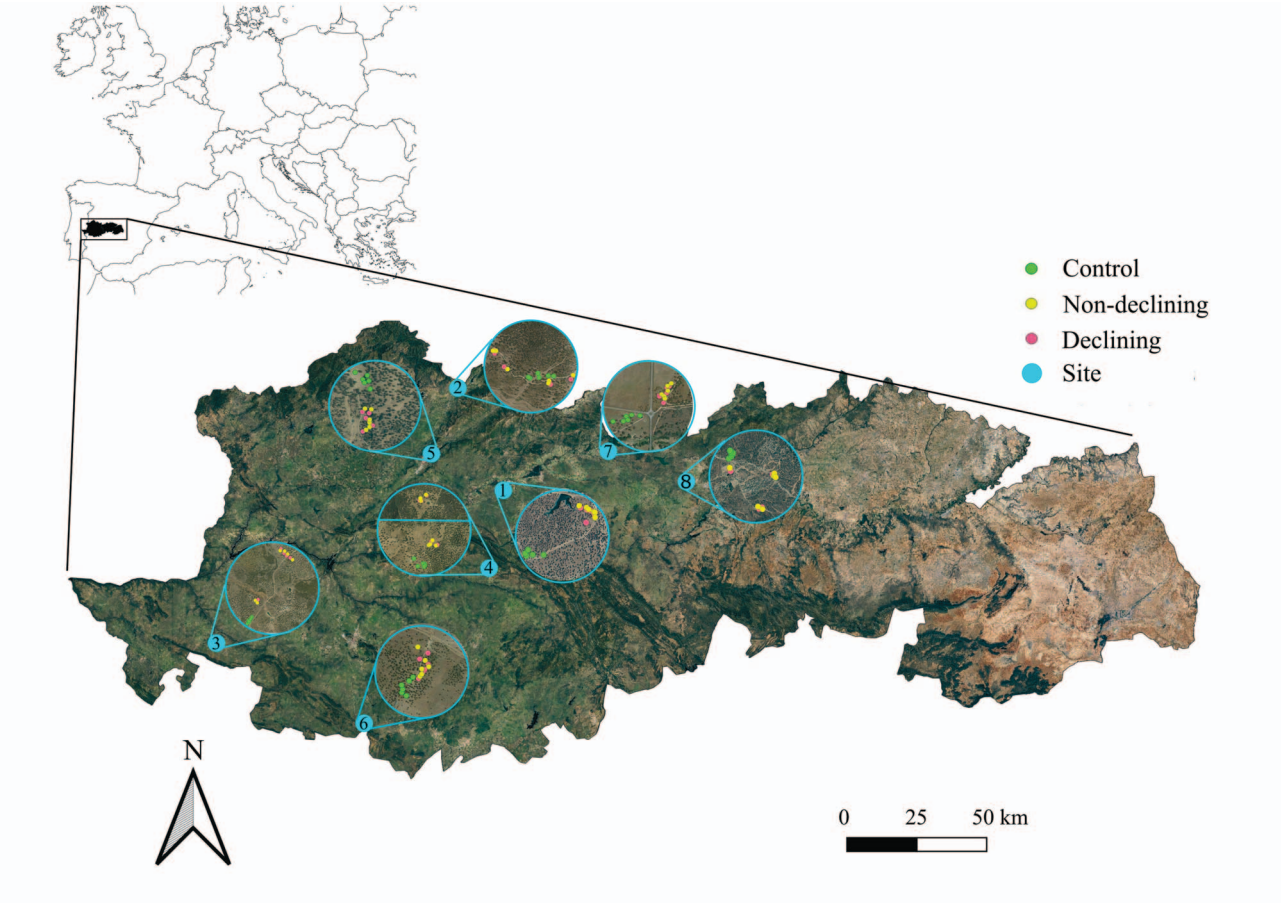

Figure 1. Location of the eight dehesa study sites (indicated with blue circles) within the central–western area of the Iberian Peninsula (the location within Europe is indicated in the upper map). The sampling design included 18 holm oak individuals per each study site: six control holm oak trees from healthy areas (marked with green points), six non-declining holm oak trees from diseased areas (marked with yellow points) and six declining holm oak trees from diseased areas (marked with red points). Google Earth Pro 7.3.3.7786 (July 21, 2020) Spain. 39° 40' 44" N , 5° 25'40"W, Eye alt 419 km. Landsat/Copernicus. Google 2020. https://www.google.com/intl/es/earth/ [February 2020].

classes to determine canopy openness. Final relative irradiance values were expressed in percentages (Esteban et al. 2007).

Chlorophyll a fluorescence induction analyses

In July 2019, from each selected healthy and declining holm oak tree, we sampled branches with 2 to 3-year-old fully expanded mature leaves. This was a criterion to make uniform and standardize the response, because holm oaks may retain their leaves for up to 3 years (Montserrat-Martí et al. 2009), and photosynthetic capacity is strongly affected by leaf age (Niinemets et al. 2005). We analyzed their photochemical efficiency and chlorophyll *a* fluorescence induction (OJIP). Specifically, four branches were sampled from the four cardinal directions, at approximately 3 m height, and one fully expanded leaf from was randomly collected. They were immediately stored in hermetic plastic bags, where relative humidity and temperatures were maintained constant, and kept in darkness for 6 h. This 'artificial predawn' (Tausz et al. 2003, Esteban et al. 2007) allowed the complete relaxation of the photosynthetic reaction centres and provided comparable conditions (due to logistics, more details in photosynthetic pigments and tocopherols analysis), a process needed to correctly determine the minimum level of fluorescence (F_o). Measurements were then performed in darkness, at room temperature (20 °C), using a fluorimeter (FluorPen FP 100; Photon Systems Instruments, Drasov, Czech Republic). This technique estimates the flow of energy through the photosystem II (PSII), being a highly sensitive signature of the linear electron transport flow and the photosynthetic efficiency (for detailed reviews see Strasser et al. 2000, Stirbet and Govindjee 2011). Excitation via blue light-emitting diodes (455 nm), optically filtered to provide a light intensity of 3000 μmol photons m^{-2} s^{-1}, allow to record fluorescence transients during 2 s at a frequency of 10 μs, 100 μs, 1 ms and 10 ms for time intervals of 10–600 μs, 0.6–14 ms, 14–100 ms and 0.1–2 s, respectively. The fluorescence values at 40 μs (F_o, step O, all reaction centres of the PSII are open), 100 μs (F_{100}), 300 μs (F_{300}), 2 ms (step J), 30 ms (step I) and maximal (maximum level of fluorescence, F_m, step P, closure of all reaction centres) were taken into consideration for further analyses. We further calculate the chlorophyll *a* fluorescence induction parameters

(energy fluctuations and yields; more details below) from F_o and F_m and the fluorescence intensities selected at 40 μs, 100 μs, 300 μs, 2 m and 30 ms. These parameters were: (i) the relative variable chlorophyll fluorescence derived from steps I and J (i.e., V_j and V_i); (ii) specific energy fluxes per primary quinone acceptor reducing PSII centre (i.e., ABS/RC, DI_o/RC, TR_o/RC, ET_o/RC). In detail, ABS refers to the photon flux absorbed by the chlorophyll antenna pigments of the PSII. Part of this energy is dissipated, mainly as heat (DI_o). Another part of this absorbed energy is funnelled to the Reaction Centre (RC), as trapping flux (TR_o). In the reaction centre, the excitation energy is converted into redox energy by reducing the electron acceptor QA to QA^-, which is then reoxidized to QA, creating an electron transport (ET_o; Strasser et al. 2000, Hermans et al. 2003). (iii) Quantum yields and efficiencies (i.e., φ_{Po}, Ψ_o, φ_{Eo}, φ_{Do} and φ_{Pav}). These yields are directly related to the energetic fluctuations obtained from the specific fluxes per RC (Strasser et al. 2000, Hermans et al. 2003). In detail, φ_{Po}, the maximum quantum yield of primary photochemistry: represents the probability that an absorbed photon is trapped by the RC and used for primary photochemistry (it is calculated as TR_o/ABS); Ψ_o, the efficiency with which a trapped exciton can move an electron into the electron transport chain further than QA (it is calculated as ET_o/TR_o). φ_{Eo}, the quantum yield of electron transport, represents the probability that an absorbed photon moves an electron into the electron transport chain (it is calculated as ET_o/ABS); φ_{Do} is the quantum yield for energy dissipation. (iv) Finally, we calculated the performance index (Pi_{Abs}), which allows in vivo evaluation of plant performance (in terms of biophysical parameters that quantify photosynthetic energy conservation; Strasser et al. 2000). This parameter summarizes three important events: the light trapping, the quantum efficiency of reduction of QA and the efficiency of electron transport from quinone to the intersystem carriers of the electron chain (Hermans et al. 2003). Thus, this index is a useful tool to screen photosynthetic performance and characterize plant vitality under stress conditions as is sensitive to changes in antenna properties, light trapping efficiency and electron transport (Strasser et al. 2000, Hermans et al. 2003). The formulas used to calculate the above parameters plus more detailed information are provided in Table S1 available as Supplementary data at *Tree Physiology* Online.

Photosynthetic pigments and tocopherols analyses

In July 2019, from each of the 144 holm oak trees, we also sampled branches with 2 to 3-year-old fully expanded mature leaves, from the four cardinal directions, and at approx. 3 m height. These samples were used to quantify the photosynthetic pigments (carotenoids and chlorophylls) and the lipophilic antioxidants (tocopherols). Due to logistics (i.e., the eight selected dehesas were spread over a large area and were thus sampled in different days and at different hours) and to the fact that these compounds (i.e., pigments and tocopherols) exhibit a high degree of environment modulation (Esteban et al. 2015*b*), the sampled branches were kept at constant temperature and in darkness for 6 h. This pre-treatment avoided circadian effects, facilitating the comparison among different sampling study sites and dates (Fernández-Marín et al. 2019). To obtain homogenized samples at the tree level, all the leaves collected from each holm oak were pooled. Then, from each leaf, we cut four discs (hereinafter referred to as plant material for simplicity), each of them having a diameter of 3 mm. This plant material was further stored in plastic bags filled with silica gel (<10% RH; Esteban et al. 2009*a*). This is a standardized methodology, specifically designed to collect and preserve plant material, that will be used for biochemical (pigment and antioxidant) analyses from remote locations where there is no close access to liquid nitrogen or to a −80 °C freezer (Esteban et al. 2009*a*).

Once in the laboratory (UPV/EHU laboratory, Basque Country, Spain), we used the plant material to extract pigments and tocopherols following the protocol described by Fernández–Marín et al. (2018). Specifically, the extractions were made using 95% acetone and the resulting liquid was homogenized (Tissue Tearor model 965670) and then centrifuged at 16,100 *g* and 4 °C. Further on, the pellet was then resuspended in pure acetone, mixed in a vortex, and centrifuged again. Both supernatants were pooled and syringe filtered through a 0.22-μm PTFE filter (Whatman, Maidstone, UK). The extractions were performed under cold conditions (4 °C) and protecting the samples against direct light. The final quantification of the pigments and tocopherols was made using the ultra-rapid uHPLC method (Lacalle et al. 2020). For this, the extracted samples were injected into the system Acquity™ uHPLC H-Class (Waters ®, Milford, MA, USA) using a reversed-phase column (Acquity UPLC® HSS C18 SB, 100Å, 1.8 μm, 2.1 ×100 mm) and a Vanguard™ pre-column (Acquity UPLC HSS C18 SB, 1.8 μm). The photodiode detector (Acquity PDA uHPLC; Waters) was then used to detect pigments, while the tocopherols were detected by fluorescence (FLR; uHPLC Acquity, Waters). The retention times and conversion factors for carotenoids were the same as those described by Lacalle et al. (2020).

This study was focused on compounds that indicate the level of photoprotection in holm oak leaves (Esteban et al. 2015*a*). For this reason, in figures and tables, the following compounds are shown: the total chlorophyll pool expressed on leaf area basis (Chl a + b, μmol m^{-2}) and the a to b chlorophyll ratio (Chl a/b, mol mol^{-1}). Additionally, the rest of the compounds were expressed on a chlorophyll basis (mmol mol^{-1} Chl): lutein (L); lutein epoxide (Lx); β-carotene (β-Car); total xanthophyll pool (VAZ = V + A + Z); total carotenoids (t-Car = neoxanthin + V + Lx + A + L + Z + α-carotene + β-Car); and total tocopherols (t-Toc, the sum of the tocopherols isomers, i.e., β - γ + α).

Statistical analyses

To analyze how the crown condition of the trees (i.e., crown defoliation and relative irradiance) and the chlorophyll *a* fluorescence induction (V_i, V_j, φ_{Po}, Ψ_o, φ_{Eo}, φ_{Do}, φ_{Pav}, PI_{Abs}, ABS/RC, TR_o/RC, DI_o/RC, ET_oRC), pigments (Chl a + b, Chl a/b, VAZ, Lx, L, β-Car) and tocopherols (t-Toc), measured on their leaves, differed between the three health statuses (i.e., control, non-declining and declining holm oaks), we performed linear mixed-effects models (LMEs). Prior to LMEs, we checked the normality (Kolmogorov–Smirnoff test) and the homoscedasticity (Levene's test) of all response variables. When these assumptions were not met, we logarithmically transformed them. We performed individual LMEs for each response variable using the 'lme' function from the 'nlme' R package (Pinheiro et al. 2020). The fixed part of the LMEs included one of the above-mentioned response variables and the crown condition of the trees. 'Sites' were introduced as random effects. We then performed ANOVAs of either type II (when dealing with a balanced design; i.e., crown defoliation, relative irradiance, pigments, and tocopherols) or type III (when dealing with an unbalanced design; i.e., chlorophyll *a* fluorescence induction parameters) using the 'car' R package (Fox and Weisberg 2019). To further look for differences between the three health statuses, we used the 'emmeans' R package (Lenth 2020) using the Tukey correction. The residuals of the models fulfilled the normality assumption. The final coefficients of the models were estimated using the restricted maximum likelihood method (REML).

For the radar plot, we calculated the average values of the chlorophyll *a* fluorescence induction parameters for each health status and we standardized them using the control group, for which we used a value of 1, as a reference. We then plotted these values using the 'radarchart' function from the 'fmsb' R package (Nakazawa 2019). Deviations from the 1 value denote an effect in each of the chlorophyll *a* fluorescence induction parameter due to health status.

We performed Spearman correlations matrix to see how crown defoliation and relative irradiance correlated with the parameters more affected by environmental modulation, φ_{Po}, PI_{Abs}, Chl a + b, Chl a/b, VAZ, L, β-Car, t-Car, and t-Toc, using the 'rcorr' function from the 'Hmisc' R package (Harrell 2019). The results of these preliminary analyses showed that crown defoliation was the variable that best correlated with most of the considered variables (i.e., φ_{Po}, PI_{Abs}, VAZ, t-Car and t-Toc).

Based on the above-mentioned Spearman correlation results, we conducted LMEs considering PI_{Abs}, VAZ and t-Toc as a function of crown defoliation. Note that no LMEs were run considering φ_{Po} since this parameter strongly covariates with PI_{Abs}, the latter being a more integrative parameter of the photosynthetic performance (Strasser et al. 2000). Likewise, the t-Car parameter was not considered either to conduct LMEs as its relationship with crown defoliation was weak comparing with the correlation between crown defoliation and VAZ. Prior to analyses, we log transformed the PI_{Abs}, VAZ and t-Toc variables as they did not meet the normality assumption. The fixed part of the LMEs included PI_{Abs}, VAZ or t-Toc and crown defoliation, while the random part of the LMEs accounted for 'sites'. For each response variable (i.e., PI_{Abs}, VAZ and t-Toc), we run three different LMEs: lineal, logarithmic and polynomial. We did so in order to see which of these three functions better explained the fit of the PI_{Abs}, VAZ and t-Toc variables as a function of crown defoliation. We selected the best models (i.e., lineal, logarithmic or polynomial) based on the Akaike Information Criterion (AIC) and Bayesian Information Criterion (BIC). When we failed to choose the best models based on either AIC or BIC (i.e., due to no significant differences), the most parsimonious model was selected. We quantified the fit of the final selected LMEs with a pseudo-R^2 (R^2_p; Nakagawa et al. 2017), whose values represent the coefficient of determination based on the likelihood-ratio test ('r.squaredLR' function from the 'MuMIn' R package; Barton 2020). The residuals of the models fulfilled the normality assumption. The final coefficients of the models were estimated using the REML.

Based on the results of the previous described LMEs, we looked for break-point values that may be used to estimate thresholds (i.e., values that mark a significant trend change; Toms and Lesperance 2003, Vito 2008) for the fit of PI_{Abs}, VAZ and t-Toc as a function of crown defoliation. For this, we run segmented regressions using the 'segmented' function from the 'segmented' R package (Vito 2008). Break points were calculated using the 'confint.segmented' function from the 'segmented' R package (Vito 2008). As we did not find significant break-points for the PI_{Abs} and VAZ variables, we only show the results corresponding to the t-Toc variable.

Finally, we also run a Structural Equation Model (SEM) based on the results of the PI_{Abs}, VAZ and t-Toc LMEs. For this, we used the 'psem' function ('piecewiseSEM' R package; Lefcheck 2016), which allowed us to introduce random effects (i.e., in order to have a similar structure as the one used for LMEs). We run SEM to look for all possible causal-effect relationships between PI_{Abs}, VAZ, t-Toc and crown defoliation. Prior to analyses, we log transformed the PI_{Abs}, VAZ and t-Toc variables as they did not meet the normality assumption. We checked the goodness of fit of the SEM based on Fisher's C statistic, which follows a chi-squared distribution and tests if the model fits the data (P-value >0.05) or not ($P < 0.05$).

All statistical analyses were performed in R (v. 4.0.0, 2020, R Development Core Team 2020). Statistical relationships were considered significant at $P < 0.05$.

Results

Defining crown defoliation and relative irradiance to the categorized trees

Crown defoliation was found to be significantly higher for declining trees than for non-declining and control trees ($P < 0.05$) (Figure 2A). As for the relative irradiance, this variable varied significantly between all health status groups ($P < 0.05$), the declining trees having again the highest values, while the control trees showing the lowest values (Figure 2B). According to these results, the control holm oaks were the least affected by leaf loss (i.e., crown defoliation estimated to vary around 4.3 ± 0.5%; relative irradiance estimated to vary around 24.0 ± 1.0%), while the declining trees were the most affected by leaf loss (i.e., crown defoliation estimated to vary around 18.8 ± 1.7%; relative irradiance estimated to vary around 35.6 ± 1.5%).

Comparing chlorophyll a fluorescence induction response between health status

Declining holm oak trees differed significantly from the control holm oak trees in (i) the specific energy flux related with the energy dissipation (DI_o/RC), (ii) in the following quantum yields: φ_{Po}, φ_{Eo} and φ_{Do} and (iii) in the PI_{Abs} (i.e., chlorophyll *a* fluorescence induction parameters; Figure 3, Table 1). No such significant differences were found between control trees and non-declining trees, or between non-declining trees and declining trees (Figure 3, Table 1). No significant differences were found between the control, non-declining and declining holm oak trees regarding the rest of the chlorophyll *a* fluorescence induction parameters (Figure 3, Table 1). Overall, this indicates that the most affected processes affected in declining trees were the excitation energy dissipation (DI_o/RC and φ_{Do}), the maximum quantum yield of primary photochemistry (φ_{Po}), the probability that an absorbed photon moves an electron into the electron transport chain (φ_{Eo}) and the integrative parameter PI_{Abs} that indicates that declining trees showed lower energy conservation from photons absorbed to the reduction of intersystem electron acceptors.

Pigments and tocopherols responses as a function of health status

The content of chlorophylls, carotenoids and tocopherols were analyzed in the three health status categories (Table 1). Declining trees showed a lower total chlorophyll content than the control trees, while the non-declining trees showed intermediate values for this variable. The decrease in the total chlorophyll content registered by the declining trees was not reflected by the changes in the antenna size, since no significant differences regarding the Chl a/b were found between the health statuses. As regarding the xanthophylls implicated in the LxL cycle (Lx and L), declining trees showed a significantly higher content of L and a significantly lower content of Lx than control trees. However, the overall Lx + L pool did not differ significantly between health statuses (data not shown). The content of total xanthophylls from the VAZ cycle differed significantly between the trees from the diseased areas (i.e., declining and non-declining) and the trees from the healthy areas (i.e., control), with lower values in the latter group. The content of t-Toc was significantly higher for the trees from the diseased areas (i.e., declining and non-declining) than for the trees from the healthy areas (i.e., control).

The performance index, total xanthophylls and tocopherols as a function of crown defoliation

Crown defoliation showed a more significant relationship with the chlorophyll *a* fluorescence induction parameters, the pigments and the tocopherols than the relative irradiance (Figure 4). In detail, crown defoliation was negatively correlated with φ_{Po} ($r = -0.18$; $P < 0.05$) and PI_{Abs} ($r = -0.17$; $P < 0.05$) and positively correlated with relative irradiance ($r = 0.22$; $P < 0.01$), t-Car ($r = 0.24$; $P < 0.01$), total VAZ ($r = 0.31$; $P < 0.001$) and t-Toc ($r = 0.35$; $P < 0.001$) (Figure 4). As for the relative irradiance, it was only positively correlated with PI_{Abs} ($r = 0.24$; $P < 0.05$) (Figure 4). Furthermore, negative correlations were also found between PI_{Abs} and VAZ ($r = -0.24$; $P < 0.05$), and between PI_{Abs} and t-Toc ($r = -0.19$; $P < 0.005$).

The results of the LMEs (i.e., where PI_{Abs}, VAZ and t-Toc were modelled as a function of crown defoliation based on the Spearman correlations' results) showed that the model that best fitted the response of PI_{Abs} to crown defoliation, was the logarithmic model (Figure 5A, Table 2). Specifically, we found higher PI_{Abs} values for the holm oaks that showed a lower than 10% crown defoliation (i.e., mainly control trees) than for the holm oaks that showed a higher than 10% crown defoliation (i.e., mainly declining trees) (Figure 5A). The model that best fitted the response of VAZ (expressed on chlorophyll bases) to crown defoliation, was the linear one. Accordingly, VAZ increased gradually along with crown defoliation (Figure 5B, Table 2). In the case of the t-Toc variable (Figure 5C, Table 2), the model that best fitted its response to crown defoliation was the polynomial model. Furthermore, the predicted values of the segmented regression model (Figure 5C, blue line) indicated that t-Toc increased at the first defoliation phases (<8.9% crown defoliation). At this crown defoliation stage, t-Toc reached its maximum value (i.e., 344.4 mmol mol^{-1} Chl). Accordingly, we established this value as a threshold.

According to the results of the SEM (Figure 6), the decrease of PI_{Abs} would affect the increase in VAZ and t-Toc levels due to the negative effect of PI_{Abs} on the photoprotective compounds. The antioxidant t-Toc had a positive effect on defoliation. Simultaneously, VAZ increased t-Toc. Eventually, these three variables (PI_{Abs}, VAZ and t-Toc) were predictive of crown defoliation.

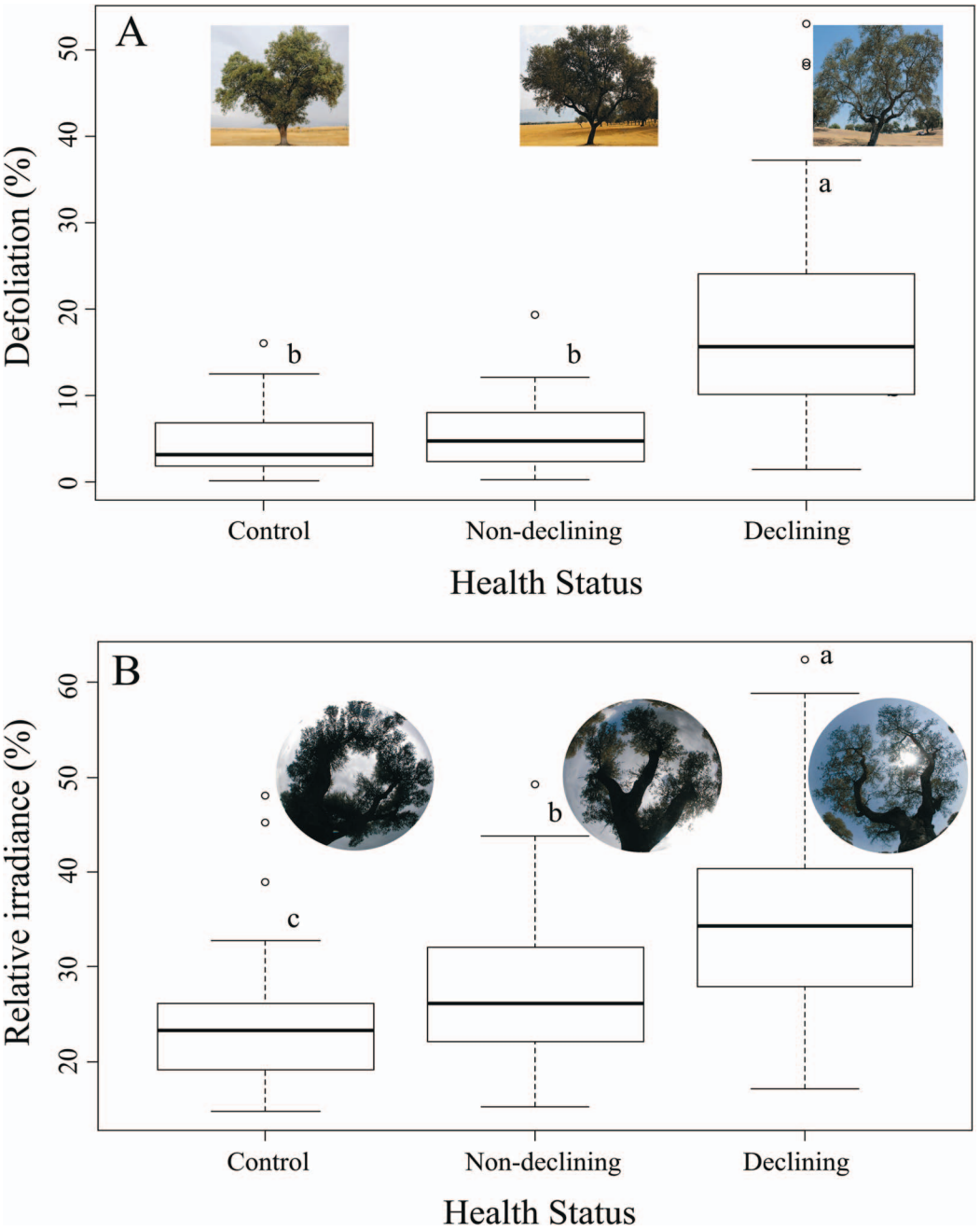

Figure 2. Boxplots showing crown defoliation (%; A) and relative irradiance (%; B) for each health status: control holm oak trees from healthy areas, non-declining holm oak trees from diseased areas, and declining holm oak trees from diseased areas. Each box represents 50% of data (n = 48 trees per each health status) distribution between the first and the third quartile; the central line represents the median; the upper and below whiskers cover the 1.5 interquartile range; empty circles represent outliers. Different letters indicate significant differences ($P < 0.05$) among control, non-declining and declining holm oak trees based on a Tukey multiple pairwise comparisons test.

Discussion

Early crown defoliation biochemical markers

Drought and pathogen infection elicit a cascade of physiological mechanisms, beginning with the oxidative stress-related signalling followed by an acclimation process or modification of a plant phenotype (decreasing the number of leaves; Ogaya and Peñuelas 2006), finally ending in crown defoliation and plant death (Vranova et al. 2002, Baier and Dietz 2005, Niinemets 2010). Crown defoliation represents just a snapshot of a decline process (de Sampaio e Paiva Camilo-Alves et al. 2013). When *P. cinnamomi* infects non-declining holm oak, trees decline relatively fast (i.e., in a few years; de Sampaio e Paiva Camilo-Alves et al. 2013), not only because this species is highly susceptible to the oomycete, but also because root rot and drought damage may act in a synergistic way. This study showed that holm oak

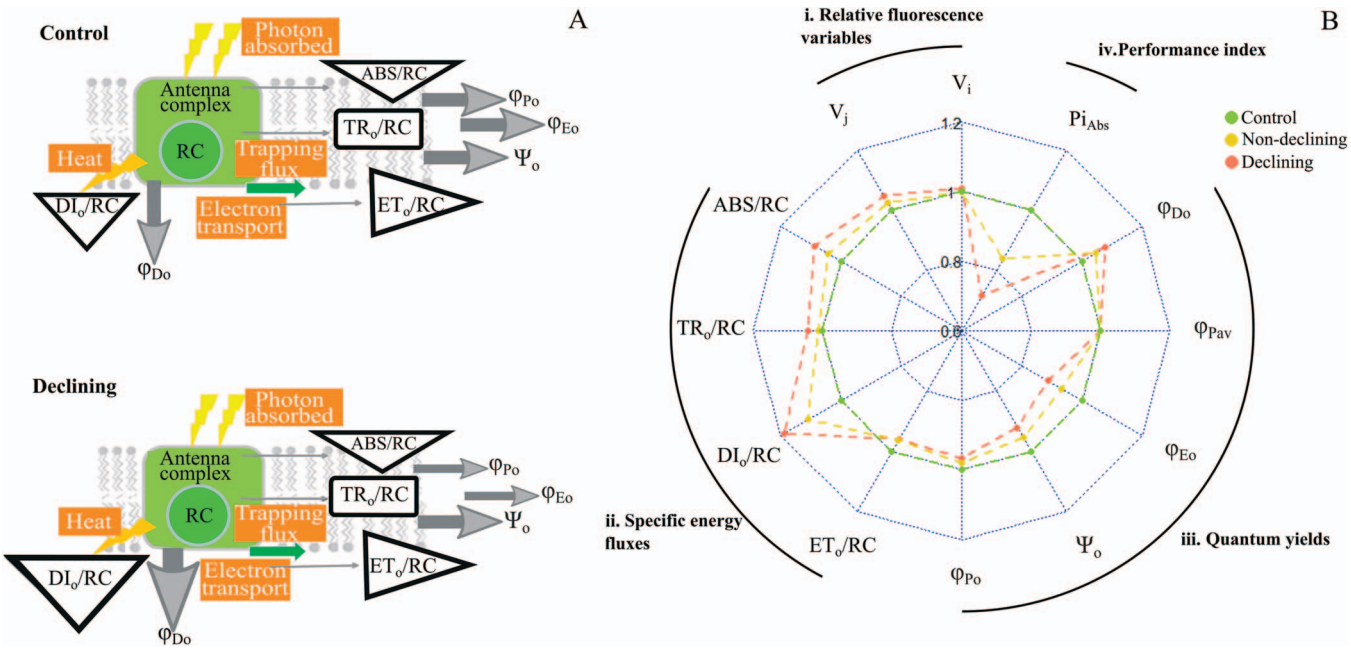

Figure 3. (A) Simplified representation of the model of energy transfer from solar light to photosynthetic electron transport in the photosynthetic apparatus (adapted from Strasser et al. 2000, Hermans et al. 2003) for control and declining trees. ABS refers to the flux of photons absorbed by the antenna complex. Part of this excitation energy is dissipated, mainly as heat (DI_o), and another part is canalized as trapping flux (TR_o) to the reaction centre (RC) and converted to redox energy and creating an electron transport (ET_o). The size of the triangles and arrows are directly proportional to the change. We only depicted significant changes based on Table 1. (B) Radar plot depicting the main chlorophyll *a* fluorescence induction parameters derived from the OJIP test ($n = 41-47$): control holm oak trees from healthy areas (marked in green), non-declining holm oak trees from diseased areas (marked in yellow) and declining holm oak trees from diseased areas (marked in red). Where (i) relative variable chlorophyll fluorescence as V_j and V_i; (ii) specific energy fluxes per primary quinone acceptor reducing PSII centres as ABS/RC, TR_o/RC, ET_o/RC and DI_o/RC, (iii) quantum yields as φ_{Po}, Ψ_o, φ_{Eo}, φ_{Do} and φ_{Pav}; and (iv) potential performance index for energy conservation (Pi_{Abs}). Note that standard error is not shown on the figure for clarity, but the coefficient of data variation was <0.7 in all cases. For further details on how the radar plot was built, refer to the section Materials and methods (cf. Statistical analyses). Definitions and formulae for all variables are given in the Materials and methods, and Table S1 available as Supplementary data at *Tree Physiology* Online.

vigour losses resulting from the stress caused by drought and/or *P. cinnamomi* root rot damage was associated with chlorophyll *a* fluorescence induction parameters (i.e., higher energy dissipation yield, φ_{Do}, DI_o/RC; lower photochemical efficiency, φ_{Po} and lower electron transport yield, φ_{Eo}; Figure 3, Table 1). This specific regulation of the photosynthetic apparatus function is in line with the specific adjustments showed by leaf-associated photoprotection compounds (i.e., Chl a + b, VAZ, Lx, L, t-Toc; Table 1). Similar upregulations in lipophilic photoprotective defences, such as the xanthophyll pool pigments (VAZ and LxL) (Hormaetxe et al. 2007, Peguero-Pina et al. 2008, Esteban et al. 2015*a*) and the tocopherols (Munné-Bosch and Alegre 2000, Hormaetxe et al. 2007, García-Plazaola et al. 2008, Fernández-Marín et al. 2017), have been previously reported for Mediterranean evergreen species. Our results thus reinforce the idea that such reactions at the leaf level are common acclimation responses to the harsh summer cocktail of unfavourable conditions that characterize the Mediterranean regions by thylakoid stabilization (Havaux et al. 2005), energy dissipation (indicated by φ_{Do}) by the operation of VAZ and LxL cycles (Demmig-Adams et al. 1999, Li et al. 2009, Esteban et al. 2015*a*) and/or antioxidant activity (Havaux et al. 2005, Dall'osto et al. 2006, Havaux and García-Plazaola 2014).

A stress marker may be any variable that correlates with plant stress (Fenollosa and Munné-Bosch 2018). Accordingly, any of the biochemical compounds implicated in the holm oak leaf-level reactions explained above fit within the definition of stress markers, which could indicate deeper damages in the plant physiological performance that may lead to irreversible defoliation processes and ultimately to the death of the individual. According to our results, the parameters that correlated well with crown defoliation could be considered as markers (i.e., mainly VAZ and t-Toc) of early decline since their response, triggered by drought stress, preceded crown defoliation. In this sense, the visually non-declining holm oaks from the diseased areas may give us important clues regarding tolerance strategies and may further serve to define early stress biomarkers. In this regard, at the early stages of tree vigour losses, when rates of defoliation are low (≈10%; Figure 2), we found significant differences in the VAZ and t-Toc pools (expressed on a chlorophyll basis; Table 1) between the holm oak trees from the diseased areas (with no differences between declining and non-declining trees)

Table 1. Physiological variables for each health status: control holm oak trees from healthy areas, non-declining holm oak trees from diseased areas and declining holm oak trees from diseased areas: (i) chlorophyll a fluorescence induction parameters derived from the OJIP test ($n = 42–47 \pm$ SE): relative variable chlorophyll fluorescence (V_j and V_i); quantum yields (φ_{Po}, Ψ_o, φ_{Eo} and φ_{Do}, and φ_{Pav}); specific energy fluxes per primary quinone acceptor reducing PSII centres (ABS/RC, TR_o/RC, ET_o/RC and DI_o/RC); potential performance index for energy conservation (Pi_{Abs}); (ii) pigments and tocopherols ($n = 48 \pm$ SE): total chlorophyll pool (Chl a + b, μmol m^{-2}), a to b chlorophyll ratio (Chl a/b, mol mol^{-1}), lutein epoxide (Lx, mmol mol^{-1} Chl), β-carotene (β-Car, mmol mol^{-1} Chl), total xanthophyll cycle pool (VAZ, mmol mol^{-1} Chl), and total tocopherols (t-Toc, mmol mol^{-1} Chl). Asterisks (*$P < 0.05$; **$P < 0.01$; ***$P < 0.001$) represent statistically significant differences according to the LMEs results. Different letters indicate significant differences ($P < 0.05$) between the three health status based on the post hoc estimated marginal means test using the Tukey correction.

	Health status			*P*-value
Variables	Control	Non-declining	Declining	
Chlorophyll *a* fluorescence induction parameters				
V_i	0.76±0.01	0.76±0.01	0.77±0.01	0.869
V_j	0.63±0.01	0.65±0.01	0.66±0.01	0.113
ABS/RC	1.43±0.03	1.40±0.06	1.55±0.05	0.089
TR_o/RC	0.98±0.02	0.99±0.02	1.02±0.02	0.304
DI_o/RC	0.45±0.02^a	0.5±0.04^{ab}	0.53±0.03^b	0.032*
ET_o/RC	0.36±0.01	0.34±0.01	0.34±0.01	0.453
φ_{Po}	0.69±0.01^a	0.68±0.01^{ab}	0.67±0.01^b	0.048*
Ψ_o	0.37±0.01	0.35±0.01	0.34±0.01	0.113
φ_{Eo}	0.25±0.01^a	0.24±0.01^{ab}	0.23±0.01^b	0.038*
φ_{Pav}	958.54±1.65	957.22±1.6	958.36±1.59	0.663
φ_{Do}	0.31±0.01^a	0.32±0.01^{ab}	0.33±0.01^b	0.021*
Pi_{Abs}	1.08±0.11^a	0.91±0.09^{ab}	0.78±0.07^b	0.023*
Pigments and tocopherols				
Chl a + b	692.28±28.35^a	626.89±19.29^{ab}	604.21±23.43^b	0.005**
Chl a/b	2.52±0.03	2.5±0.03	2.46±0.04	0.190
VAZ	25.33±1.18^a	29.1±1.41^b	32.22±1.94^b	<0.001***
Lx	1.57±0.22^a	0.81±0.11^b	0.74±0.10^b	<0.001***
L	132.89±2.23^a	137.47±1.54^{ab}	139.06±2.13^b	0.035*
β-Car	89.46±1.79	92.47±1.8	94.44±1.93	0.073
t-Car	292.85±4.31^a	304.18±3.09^b	310.73±4.11^b	<0.001***
t-Toc	185.74±15.8^a	298.41±22.16^b	357.25±24.67^b	<0.001***

*Definitions and formulae for chlorophyll *a* fluorescence induction parameters are shown in the Materials and methods section and in Table S1 available as Supplementary data at *Tree Physiology* Online.

Table 2. Results of the LMEs (i.e., the ANOVA table) in which Pi_{Abs}, VAZ and t-Toc were fitted as a function of crown defoliation. Asterisks (*$P < 0.05$; ***$P < 0.001$) indicate statistically significant relationships. R^2_p values represent the coefficient of determination based on the likelihood-ratio test (more details on the calculation in the Materials and methods section) (degrees of freedom, Df; standard error, SE; potential performance index for energy conservation, Pi_{Abs}; total xanthophyll cycle pool, VAZ; total tocopherols, t-Toc).

Fixed effects	Df (numerator)	Df (denominator)	Estimate	SE	*F*	*P*-value	R^2_p
Pi_{Abs} as function of defoliation							0.168
Intercept	1	121	−0.112	0.122	5.51	0.025*	
Log (defoliation)	1	121	−0.077	0.038	3.98	0.048*	
VAZ as function of defoliation							0.439
Intercept	1	135	3.225	0.094	1277.25	<0.001***	
Defoliation	1	135	0.007	0.002	12.72	<0.001***	
t-Toc as function of defoliation							0.206
Intercept	1	134	4.659	0.209	2909.13	<0.001***	
Defoliation	1	134	−0.052	0.018	4.47	0.036*	
$\sqrt{}$Defoliation	1	134	0.464	0.126	13.56	<0.001***	

and the holm oak trees from the healthy areas (i.e., control trees). These findings suggest that the compounds induced in the leaves of the non-declining trees (i.e., both VAZ and t-Toc) could be assessed as early indicators of defoliation as they appear before the characteristic tipping points of crown defoliation that define the onset of holm oak decline and death.

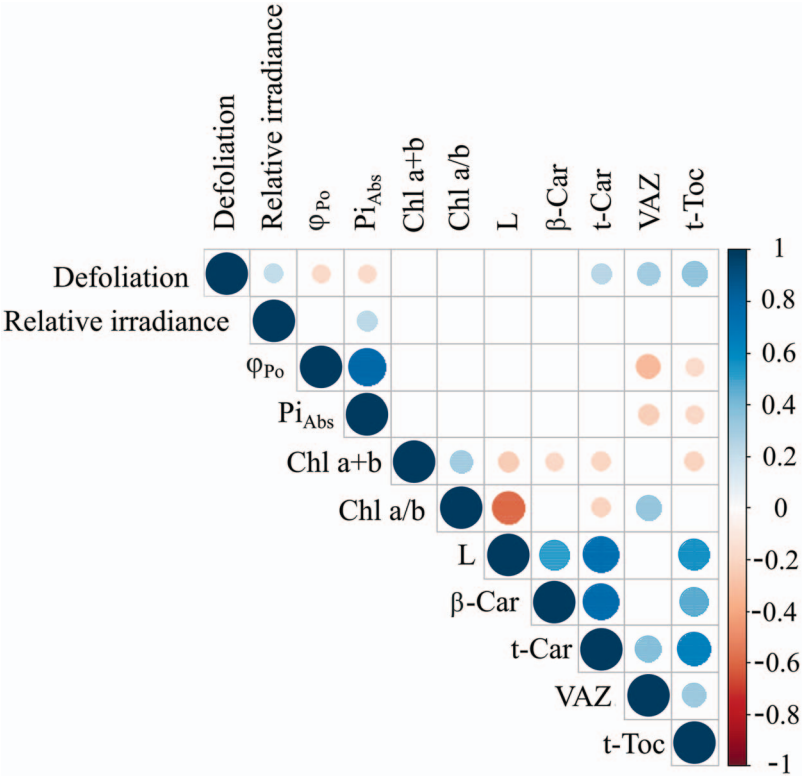

Figure 4. Spearman's rank correlation matrix plot showing the relationship between: (i) crown assessment variables (defoliation (%) and relative irradiance (%)); (ii) chlorophyll *a* fluorescence induction parameters derived from the OJIP test (photochemical efficiency (φ_{Po}) and potential performance index for energy conservation (Pi_{Abs}); (iii) pigments (total chlorophyll pool (Chl a + b, μmol m^{-2}), a to b chlorophyll ratio (Chl a/b, mol mol^{-1}), lutein (L, mmol mol^{-1} Chl), β-carotene (β-Car, mmol mol^{-1} Chl), total xanthophyll pool (VAZ, mmol mol^{-1} Chl), total carotenoid pool (t-Car, mmol mol^{-1} Chl); and (iv) total tocopherols (t-Toc, mmol mol^{-1} Chl). Negative and positive correlations are indicated in red and blue, respectively. The strength of the correlation is indicated by dot size and colour saturation. Note that only significant correlations are shown ($P < 0.05$).

The physiological threshold to predict plant performance

As both t-Toc and VAZ pigments are subjected to environmental modulation, we found a positive correlation between them (Figure 4), suggesting that both act synergistically to prevent damages at the leaf-level caused by stress factors. Changes of both pools of photoprotective compounds, under environmental stress, seem to usually display a highly synchronized mode (Garcia-Plazaola et al. 2004, Munné-Bosch 2005, Havaux and García-Plazaola 2014). This synchrony indicates a synergistic and complementary function as controllers of membrane fluidity and photoprotection (Havaux et al. 2005, Esteban et al. 2009*b*). However, when modelling t-Toc and VAZ as a function of crown defoliation, we found a continuous rise of VAZ content and a non-linear saturated curve for t-Toc (Figure 5). These reactions respond to their differential role in the biochemical adjustments that the photosynthetic apparatus undergoes (Anderson et al. 2008, Esteban et al. 2015*a*). Explicitly, in the case of the xanthophylls (VAZ pigments), and considering the PSII antenna proteins constricted composition, the linear fit as a function of crown defoliation (Figure 5B) supports the presence of a free pool of VAZ xanthophylls in the thylakoid membranes (Havaux and García-Plazaola 2014, Esteban et al. 2015*a*) and/or indicates that this extra pool of VAZ pigments is bound to stress proteins such as early light-induced proteins that are upregulated in response to unfavourable conditions (Alamillo and Bartels 2001, Zarter et al. 2006). Conversely, at the onset of the crown defoliation process, a quick rise in t-Toc occurred, reaching its maximum threshold level when declining symptoms (crown defoliation) were already evident (8.9% defoliation) and descending afterword along with the increase of crown defoliation. Most of this newly formed t-Toc pool is probably sequestered in plastoglobules (Vidi et al. 2006), dynamically exchanging with the thylakoid t-Toc pool. This 'A-shaped' curve resulted from an initial activation phase to counteract the damage, followed by a decreasing second phase when the oxidative stress was too severe and t-Toc degradation exceeded the rate of recycling and synthesis de novo (Munné-Bosch 2005, Havaux and García-Plazaola 2014). Similar trends of tocopherols have been reported in previous studies (Juvany et al. 2012, 2013). Stress-tolerant plants only exhibit the initial t-Toc phase, similar to that observed for our control holm oak trees (Figure 5C, green circles). Stress-sensitive plants instead exhibit

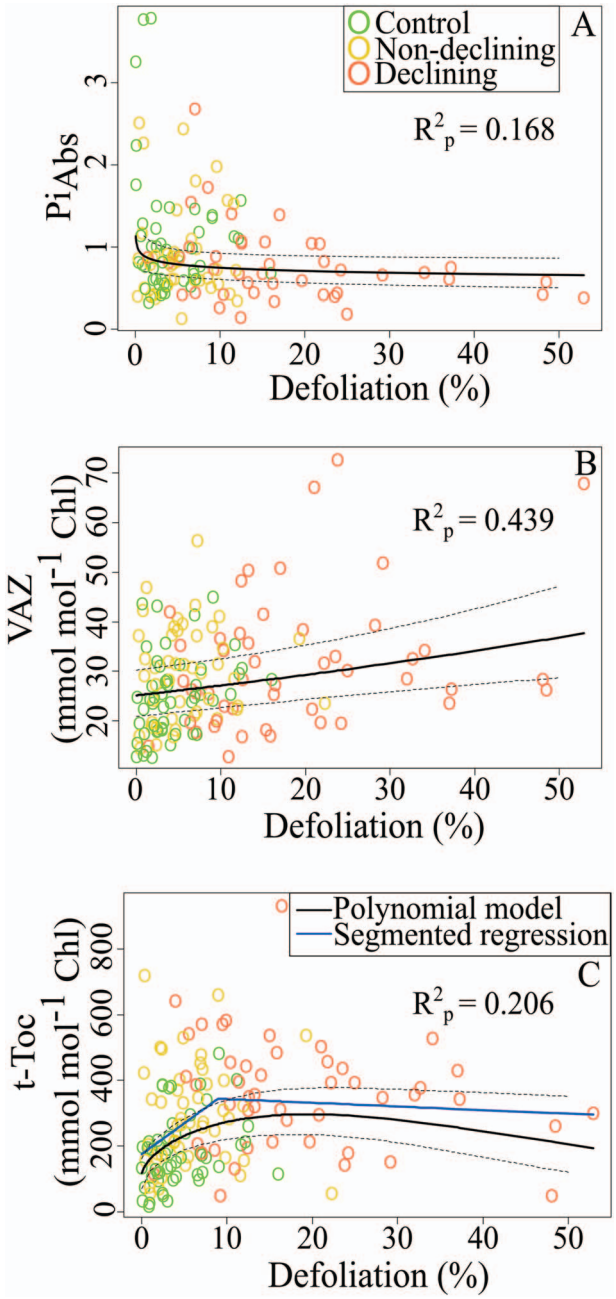

Figure 5. LME results showing Pi_{Abs} (i.e., potential performance index for energy conservation; A), VAZ (total xanthophyll pool expressed on total chlorophyll, mmol mol^{-1} Chl; B) and t-Toc (total tocopherols expressed on total chlorophyll, mmol mol^{-1} Chl; C) fits as a function of crown defoliation. Solid black lines represent fitted data, while dotted upper and lower lines represent the 95% confidence interval. In the case of t-Toc (C), the 'A-shaped' segmented regression is also represented with a blue bold line, on which the highest point represents the break point. This break point value depicts the maximum level reached by t-Toc (i.e., its threshold value) and its trend change along with crown defoliation (see Table 2 for statistics parameters). Empty circles in each plot represent the different health status: control holm oak trees from healthy areas (marked in green), non-declining holm oak trees from diseased areas (marked in yellow) and declining holm oak trees from diseased areas (marked in red). For each variable, we show the R^2_p; measuring the fraction of variation explained by the model (Nakagawa et al. 2017).

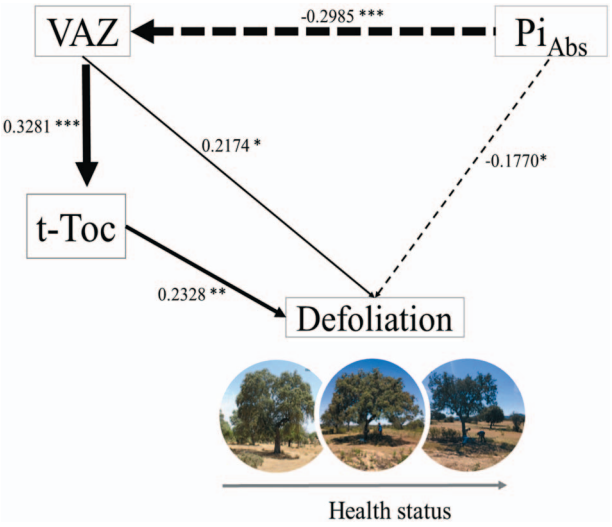

Figure 6. SEM results. Path diagram representing hypothesized causal-effect relationships between crown defoliation, photoprotective compounds (i.e., total xanthophyll pool, VAZ, mmol mol^{-1} Chl; and total tocopherols, t-Toc, mmol mol^{-1} Chl) and potential performance index for energy conservation (i.e., Pi_{Abs}, formula available in Table S1 available as Supplementary data at *Tree Physiology* Online). Note that all variables were logarithmically transformed prior to analyses. Causal-effect relationships are indicated by arrows as follows: positive and negative effects are indicated by solid and dashed lines, respectively, and the line thickness represents the weakness or strength of the relationship. Numbers indicate the standardized estimated regression weights. All the relationships represented are significant. Asterisks represent statistically significant differences ($^*P < 0.05$; $^{**}P < 0.01$; $^{***}P < 0.001$).

the decreasing collapse phase (Munné-Bosch 2005), similar to the observed in the declining holm oak trees included in our study (Figure 5C, red circles). This indicates that a senescence non-reversible process (probably related to signalling role and remobilization phase) may be occurring in declining holm oak trees. Hence, our segmented regression model, which linked early markers with a tree health status gradient (based on crown defoliation; Figure 5C), provided us with the opportunity to find a threshold t-Toc value (i.e., 344.4 mmol mol^{-1} Chl) that marks the onset of the non-reversible declining phase.

The mechanistic model

We propose a mechanistic process that may predict crown defoliation based on the causal-effect relationships that we found between Pi_{Abs} and the photoprotective compounds (VAZ and t-Toc), especially at the early stages of tree defoliation (Figure 6). Specifically, at low crown defoliation levels (<10%), we observed a down-regulation of the photochemical efficiency ($\varphi_{Po} \approx 0.7$) associated with defoliation, since in declining trees, φ_{Po} and Pi_{Abs} were significantly lower than in the control holm oak trees from the healthy areas. Down-regulation of the photochemical efficiency could be associated with a decrease in carbon assimilation (Gratani and Bombelli 2000) as, during the summertime, the diffusion of CO_2 from the atmosphere to the

carboxylation sites in leaves may experience greater resistance due to stomata closure (Nogués et al. 2014). However, the lower values of photosynthetic efficiency found for the declining trees ($\varphi_{Po} < 0.68$) could be explained by a lower electron transport rate (Strasser et al. 2000, indicated by the parameter φ_{Eo}) possibly leading to the activation of photoprotective responses (Bussotti et al. 2011) triggered by the increase in leaf concentration of LxL, VAZ and t-Toc (Table 1, Figure 5).

The question that now arises is whether the reactions of these compounds (VAZ and t-Toc) are induced at the onset of the tree decline process ('damage response') or are a part of the photoacclimation process ('tolerance response') in response to water stress. Based on our results (i.e., Figures 4 and 6) these reactions may be interpreted more as a photoacclimation process ('tolerance response') rather than as a 'damage response' (García-Plazaola et al. 2008). This photoacclimation process agrees with literature that reports holm oak photoprotective responses to drought stress (Canadell et al. 1992), which seems to be part of a conservative resource-use strategy of this species (i.e., low responsiveness to changes in environmental conditions and scarce use of available resources). Similar patterns have been found for other evergreen woody species and seem to allow them to adapt and tolerate the harsh Mediterranean conditions and avoid the use of deficient resources once conditions reach stressful levels (Valladares et al. 2000). Moreover, photoprotective responses acquired during stressful conditions may confer them more tolerance and resistance to face subsequent stressful factors and conditions not only at the tree-level but also at within-population level (Matesanz and Valladares 2014). Nevertheless, based on our results, we may also take into consideration the presence of a photooxidative damage in trees at advanced defoliation stages ('damage response') where the t-Toc trend dropped down (Munné-Bosch 2005). This decrease may be attributed to the deficiency of t-Toc recycling by ascorbate due to the possible lack of carbohydrates for its synthesis (Tausz et al. 2004, García-Plazaola et al. 2008). As biochemical and diffusion limitations of photosynthesis-related with leaf age have been described for *Q. ilex* (Niinemets et al. 2005), the declining process observed in this study could be related to age-associated increased biochemical limitation (Niinemets et al. 2005). Overall, the reduction of leaf longevity, simulating premature aging, would imply a decreasing number of leaves (Ogaya and Peñuelas 2006) and shifts in branching and shoot length (as has been described for conifers; Niinemets and Lukjanova 2003), causing shorter current-year shoots (Ogaya and Peñuelas 2006) that may counteract for the overall canopy depletion in declining holm oaks. Overall, further research will be needed to confirm to what extent the observed leaf-level physiological adjustments preceding defoliation could be a consequence of damage or of acclimation and tolerance. Disentangling shoot bifurcation rates (Niinemets and Lukjanova 2003) and canopy dynamics could provide insights into the defoliation process at the whole-plant level. Hence, controlled experiments in which trees' health status and their physiological responses to drought are monitored over time are thus needed to address these complex questions.

Final remarks and conclusions

Early photoprotective responses to stress, reflected in the variations of the photoprotective compounds (mainly VAZ and t-Toc), represent a conservative resource-use strategy that allows holm oak to survive in the harsh Mediterranean conditions. These responses preceded crown defoliation, the most radical response to stress and a tipping point of no recovery for holm oak. We identified early markers of stress that may be used as a useful diagnostic tool given that drought and pathogen incidence are expected to enhance holm oak decline (Brasier 1996, Resco De Dios et al. 2007, Lindner et al. 2010, Natalini et al. 2016). Accordingly, the results presented in this study may provide basic knowledge to elaborate preventive measures and adaptive strategies (Pollastrini et al. 2016) intended to prevent both the appearance and the propagation of declining foci in the dehesa ecosystems. The early stress markers implemented here could be more easily estimated by remote sensing techniques (i.e., hyperspectral and thermal images), currently used to diagnose the health status of trees at a landscape level (Gamon et al. 2016, Zarco-Tejada et al. 2018, Ensminger 2020). Indeed, the Earth Explorer Fluorescence Explorer mission that will map fluorescence vegetation (our site 1 will be included) will greatly expand the potential of these early markers in the near future to track forest decline incidence (Hernández-Clemente et al. 2019) and to facilitate the adoption of preventive measures that may counterbalance the effects of drought and pathogens on trees.

Supplementary data

Supplementary data for this article are available at *Tree Physiology* Online.

Data and materials availability

Data for this article are available at *Tree Physiology* Online.

Conflict of interest

None declared.

Authors' contributions

Research conception and design were by R.E. and J.C.Y., methodology implementation by M.E.-V. and R.E., experiment execution and data collection by M.E.-V., R.E., U.A. and M.V., data analysis/interpretation by M.E.-V., R.E., J.C.Y. and A.-M.H., data

discussion by M.E.-V., R.E., A.-M.H., M.V., A.S., G.M. and J.C.Y., manuscript draft writing by M.E.-V., R.E., A.–M.H. and J.C.Y., and final writing and revision by M.E.-V., R.E., J.M.B., J.I.G.P., M.V., A.S., G.M., J.C.Y. and A.-M.H.

Acknowledgments

We thank Dr Víctor Rolo Romero for help during sampling. We also acknowledge the private owners for facilitating access to the sampling sites. Thanks to Celia López-Carrasco Fernández and the "Consejería de Agricultura, Medioambiente y Desarrollo rural de la Junta de Castilla-la Mancha" for logistical support during the field-work and for allowing two of their experimental sites to be used for this study.

Funding

This research was mainly funded by the Spanish Government through the IBERYCA project (CGL2017-84723-P) and its associated FPI scholarship BES-2014-067971 (to M.E.-V.). It was further supported by the BC3 María de Maeztu excellence accreditation (MDM-2017-0714; the Spanish Government) and by the BERC 2018-2021 and the UPV/EHU-GV IT-1018-16 program (Basque Government). Additionally, this research was further supported through the 'Juan de la Cierva program' (the Spanish Government to M.V.; (IJCI-2017-34640).) and two projects funded by the Romanian Ministry of Education and Research through UEFISCDI (NATIvE, PN-III-P1-1.1-PD-2016-0583 and REASONING, PN-III-P1-1.1-TE-2019-1099 to A.-M.H.).

References

Alamillo JM, Bartels D (2001) Effects of desiccation on photosynthesis pigments and the ELIP-like dsp 22 protein complexes in the resurrection plant *Craterostigma plantagineum*. Plant Sci 160:1161–1170.

Allen CD, Macalady AK, Chenchouni H, et al. (2010) A global overview of drought and heat-induced tree mortality reveals emerging climate change risks for forests. For Ecol Manage 259:660–684.

Anderegg W, Kane JM, Anderegg L (2013) Consequences of widespread tree mortality triggered by drought and temperature stress. Nat Clim Chang 3:30–36.

Anderson JM, Chow WS, De Las Rivas J (2008) Dynamic flexibility in the structure and function of photosystem II in higher plant thylakoid membranes: The grana enigma. Photosynth Res 98:575–587.

Baier M, Dietz KJ (2005) Chloroplasts as source and target of cellular redox regulation: a discussion on chloroplast redox signals in the context of plant physiology. J Exp Bot 56:1449–1462.

Barton K (2020) Package 'MuMIn' *Title Multi-Model Inference*. R Package version 14317. https://cran.r-project.org/package=MuMIn (11 May 2020, date last accessed).

Bellard C, Leclerc C, Leroy B, Bakkenes M, Veloz S, Thuiller W, Courchamp F (2014) Vulnerability of biodiversity hotspots to global change. Glob Ecol Biogeogr 23:1376–1386.

Bonan G (2016) Forests, climate, and public policy: A 500-year interdisciplinary odyssey. Annu Rev Ecol Evol Syst 47:97–121.

Brasier CM (1996) *Phytophthora cinnamomi* and oak decline in southern Europe environmental constraints including climate change. Ann Sci For 53:346–358.

Breshears DD, López-Hoffman L, Graumlich LJ (2011) When ecosystem services crash: Preparing for big, fast, patchy climate change. Ambio 40:256–263.

Bussotti F (2004) Assessment of stress conditions in *Quercus ilex* L. leaves by O-J-I-P chlorophyll a fluorescence analysis. Plant Biosyst 138:101–109.

Bussotti F, Desotgiu R, Cascio C et al. (2011) Ozone stress in woody plants assessed with chlorophyll a fluorescence. A critical reassessment of existing data. Environ Exp Bot 73:19–30.

Camarero JJ, Olano JM, Jackeline S, Alfaro A, Fernández-Marín B, Becerril JM, García-Plazaola I (2012) Photoprotection mechanisms in *Quercus ilex* under contrasting climatic conditions. Flora 207: 557–564.

Canadell J, Djema A, López B, Lloret F, Sabate S, Siscart D, Gracia C (1992) 4.1 Structure and dynamics of the root system. In: Roda F, Retana J, Gracia CA, Bellot J (eds) Ecology of Mediterranean evergreen oak forest. Springer-Verlag, Berlin Heidelberg, pp 1689–1699.

Carnicer J, Coll M, Ninyerola M, Pons X, Sánchez G, Peñuelas J (2011) Widespread crown condition decline, food web disruption, and amplified tree mortality with increased climate change-type drought. Proc Natl Acad Sci USA 108:1474–1478.

Corcobado-Sánchez T (2013) Influencia de *Phytophthora cinnamomi* Rands en el decaimiento de *Quercus ilex* L. y su relación con las propiedades del suelo y las ectomicorrizas (Doctoral dissertation), University of Extremadura, Plasencia, http://dehesa.unex.es/handle/10662/689.

Corcobado T, Solla A, Madeira MA, Moreno G (2013) Combined effects of soil properties and *Phytophthora cinnamomi* infections on *Quercus ilex* decline. Plant Soil 373:403–413.

Corcobado T, Vivas M, Moreno G, Solla A (2014) Ectomycorrhizal symbiosis in declining and non-declining *Quercus ilex* trees infected with or free of *Phytophthora cinnamomi*. For Ecol Manage 324: 72–80.

Curiel Yuste J, Flores-Rentería D, García-Angulo D, Hereş A-M, Bragă C, Petritan A-M, Petritan IC (2019) Cascading effects associated with climate-change-induced conifer mortality in mountain temperate forests result in hot-spots of soil CO2 emissions. Soil Biol Biochem 133:50–59.

Dall'osto L, Lico C, Alric J, Giuliano G, Havaux M, Bassi R (2006) Lutein is needed for efficient chlorophyll triplet quenching in the major LHCII antenna complex of higher plants and effective photoprotection in vivo under strong light. BMC Plant Biol 6:32.

Demmig-Adams B, Adams WW, Ebbert V, Logan BA (1999) Ecophysiology of the xanthophyll cycle. In: Frank HA, Young AJ, Britton G, Cogdell RJ (eds) The photochemistry of carotenoids. Springer, Dordrecht, pp 245–269.

de Sampaio e Paiva Camilo-Alves C, da Clara M, de Almeida Ribeiro N (2013) Decline of Mediterranean oak trees and its association with *Phytophthora cinnamomi*: A review. Artic Eur J For Res 132:411–432.

Ensminger I (2020) Fast track diagnostics: hyperspectral reflectance differentiates disease from drought stress in trees. Tree Physiol 40:1143–1146.

Esteban R, García-Plazaola JI (2014) Involvement of a second xanthophyll cycle in non-photochemical quenching of chlorophyll fluorescence: The lutein epoxide story. In: Demmig-Adams B, Garab G, Govindjee WA (eds) Non-photochemical quenching and energy dissipation in plants, algae and cyanobacteria, advances in photosynthesis and respiration. Springer, Dordrecht, pp 277–295.

Esteban R, Jiménez E, Jiménez MS, Morales D, Hormaetxe K, Becerril JM, García-Plazaola JI (2007) Dynamics of violaxanthin and lutein

epoxide xanthophyll cycles in Lauraceae tree species under field conditions. Tree Physiol 27:1407–1414.

Esteban R, Balaguer L, Manrique E et al. (2009*a*) Alternative methods for sampling and preservation of photosynthetic pigments and tocopherols in plant material from remote locations. Photosynth Res 101:77–88.

Esteban R, Olano J, Castresana J, Fernández-Marín B, Hernández A, Becerril J, García-Plazaola JI (2009*b*) Distribution and evolutionary trends of photoprotective isoprenoids (xanthophylls and tocopherols) within the plant kingdom. Physiol Plant 135:379–389.

Esteban R, Fernández-Marín B, Olano JM, Becerril JM, García-Plazaola JI (2014) Does plant colour matter? Wax accumulation as an indicator of decline in *Juniperus thurifera*. Tree Physiol 34: 267–274.

Esteban R, Barrutia O, Artetxe U, Fernández-Marín B, Hernández A, García-Plazaola JI (2015*a*) Internal and external factors affecting photosynthetic pigment composition in plants: A meta-analytical approach. New Phytol 206:268–280.

Esteban R, Moran JF, Becerril JM, García-Plazaola JI (2015*b*) Versatility of carotenoids: An integrated view on diversity, evolution, functional roles and environmental interactions. Environ Exp Bot 119: 63–75.

Fenollosa E, Munné-Bosch S (2018) Photoprotection and photooxidative stress markers as useful tools to unravel plant invasion success. In: Sánchez-Moreiras AM, Reigosa MJ (eds) Advances in plant ecophysiology techniques. Springer, Cham, pp 153–175.

Fernández-Marín B, Gago J, Clemente-Moreno MJ, Flexas J, Gulías J, García-Plazaola JI (2019) Plant pigment cycles in the high-Arctic Spitsbergen. Polar Biol 42:675–684.

Fernández-Marín B, García-Plazaola JI, Hernández A, Esteban R (2018) Plant photosynthetic pigments: methods and tricks for correct quantification and identification. In: Sánchez-Moreiras AM, Reigosa MJ (eds) Advances in plant ecophysiology techniques. Springer, Cham, pp 29–50.

Fernández-Marín B, Hernández A, Garcia-Plazaola JI, Esteban R, Míguez F, Artetxe U, Gómez-Sagasti MT (2017) Photoprotective strategies of Mediterranean plants in relation to morphological traits and natural environmental pressure: A meta-analytical approach. Front Plant Sci 8:1051.

Ferreira T, Rasband W (2019) ImageJ User Guide ImageJ User Guide IJ 1.46r. imagej.nih.gov/ij/docs/guide/ (21 September 2020, date last accessed).

Fox J, Weisberg S (2019) An R companion to applied regression. Third Edn, Sage, Thousand Oaks, CA. https://socialsciences.mcmaster.ca/jfox/Books/Companion/ (27 May 2020, date last accessed).

Frazer GW, Canham CD, Lertzman KP (1999) Gap light analyzer (gla): imaging software to extract canopy structure and gap light transmission indices from true-colour fisheye photographs, users manual and program documentation. Copyright © 1999: Simon Fraser University, Burnaby, British Columbia, and the Institute of Ecosystem Studies, Millbrook, New York.

Gallego FJ, Perez De Algaba A, Fernandez-Escobar R (1999) Etiology of oak decline in Spain. Eur J For Pathol 29:17–27.

Gamon JA, Huemmrich KF, Wong CYS, Ensminger I, Garrity S, Hollinger DY, Noormets A, Peñuelas J (2016) A remotely sensed pigment index reveals photosynthetic phenology in evergreen conifers. Proc Natl Acad Sci, USA 113:13087–13092.

García-Angulo D, Hereş A-M, Fernández-López M, Flores O, Sanz M, Rey A, Valladares F, Curiel Yuste J (2020) Holm oak decline and mortality exacerbates drought effects on soil biogeochemical cycling and soil microbial communities across a climactic gradient, unpublished manuscript. Soil Biol Biochem 149:107921.

García-Plazaola JI, Becerril JM (2001) Seasonal changes in photosynthetic pigments and antioxidants in beech (*Fagus sylvatica*) in a Mediterranean climate: Implications for tree decline diagnosis. Aust J Plant Physiol 28:225–232.

Garcia-Plazaola JI, Becerril JM, Hernandez A, Niinemets U, Kollist H (2004) Acclimation of antioxidant pools to the light environment in a natural forest canopy. New Phytol 163:87–97.

García-Plazaola JI, Esteban R, Hormaetxe K, Fernández-Marín B, Becerril JM (2008) Photoprotective responses of Mediterranean and Atlantic trees to the extreme heat-wave of summer 2003 in Southwestern Europe. Trees 22:385–392.

Gazol A, Sangüesa-Barreda G, Camarero JJ (2020) Forecasting forest vulnerability to drought in Pyrenean silver fir forests showing dieback. Front For Glob Chang 3:1–13.

Gómez-Aparicio L, Ibáñez B, Serrano MS, De Vita P, Ávila JM, Pérez-Ramos IM, García LV, Esperanza Sánchez M, Marañón T (2012) Spatial patterns of soil pathogens in declining Mediterranean forests: implications for tree species regeneration. New Phytol 194: 1014–1024.

Gómez F, Navarro-Cerrillo R, Reports AP-L-S (2019) U (2019) Assessment of functional and structural changes of soil fungal and oomycete communities in holm oak declined dehesas through metabarcoding analysis. Sci Rep 9:1–16.

Gratani L, Bombelli A (2000) Correlation between leaf age and other leaf traits in three Mediterranean maquis shrub species: *Quercus ilex, Phillyrea latifolia* and *Cistus incanus*. Environ Exp Bot 43: 141–153.

Harrell F (2019) Hmisc: Harrell miscellaneous. R Package version 43-0. https://cran.r-project.org/package=Hmisc (27 May 2020, date last accessed).

Harris I, Osborn TJ, Jones P, Lister D (2020) Version 4 of the CRU TS monthly high-resolution gridded multivariate climate dataset. Sci Data 7:1–18.

Hartmann H, Moura CF, Anderegg WRL et al. (2018) Research frontiers for improving our understanding of drought-induced tree and forest mortality. New Phytol 218:15–28.

Havaux M, García-Plazaola JI (2014) Beyond non-photochemical fluorescence quenching: The overlapping antioxidant functions of zeaxanthin and tocopherols. In: Demmig-Adams B, Garab G, Adams W, Govindjee (eds) Non-photochemical quenching and energy dissipation in plants, algae and cyanobacteria. Springer, Dordrecht Heidelberg, New York, London, pp 584–597.

Havaux M, Eymery F, Porfirova S, Rey P, Dörmann P (2005) Vitamin E protects against photoinhibition and photooxidative stress in *Arabidopsis thaliana*. Plant Cell 17:3451–3469.

Hereş AM, Kaye MW, Granda E, Benavides R, Lázaro-Nogal A, Rubio-Casal AE, Valladares F, Curiel Yuste J (2018) Tree vigour influences secondary growth but not responsiveness to climatic variability in Holm oak. Dendrochronologia 49:68–76.

Herguido-Sevillano E, Pulido M, Lavado J, Schnabel S (2017) Spatial patterns of lost and remaining trees in the Iberian wooded rangelands. Appl Geogr 87:170–183.

Hermans C, Smeyers M, Maldonado Rodriguez R, Eyletters M, Strasser RJ, Delhaye JP (2003) Quality assessment of urban trees: A comparative study of physiological characterisation, airborne imaging and on site fluorescence monitoring by the OJIP-test. J Plant Physiol 160:81–90.

Hernández-Clemente R, Hornero A, Mottus M, Penuelas J, González-Dugo V, Jiménez JC, Suárez L, Alonso L, Zarco-Tejada PJ (2019) Early diagnosis of vegetation health from high-resolution hyperspectral and thermal imagery: lessons learned from empirical relationships and radiative transfer modelling. Curr For Rep 5:169–183.

Holland V, Koller S, Brüggemann W (2014) Insight into the photosynthetic apparatus in evergreen and deciduous European oaks during autumn senescence using OJIP fluorescence transient analysis. Plant Biol 16:801–808.

Hormaetxe K, Becerril JM, Hernández A, Esteban R, García-Plazaola JI (2007) Plasticity of photoprotective mechanisms of *Buxus sempervirens* L. leaves in response to extreme temperatures. Plant Biol 9:59–68.

Juvany M, Müller M, Munné-Bosch S (2012) Leaves of field-grown mastic trees suffer oxidative stress at the two extremes of their lifespan. J Integr Plant Biol 54:584–594.

Juvany M, Müller M, Munné-Bosch S (2013) Photo-oxidative stress in emerging and senescing leaves: a mirror image? J Exp Bot 64:3087–3098.

Lacalle RG, Aparicio JD, Artetxe U, Urionabarrenetxea E, Polti MA, Soto M, Garbisu C, Becerril JM (2020) Gentle remediation options for soil with mixed chromium (VI) and lindane pollution: biostimulation, bioaugmentation phytoremediation and vermiremediation. Heliyon 6:e04550.

Lefcheck JS (2016) piecewiseSEM: Piecewise structural equation modelling in r for ecology, evolution, and systematics. Methods Ecol Evol 7:573–579.

Lenth R (2020) emmeans: Estimated marginal means, aka least-squares means. R package version 146. https://cran.r-project.org/package=emmeans (27 May 2020, date last accessed).

Li Z, Ahn TK, Avenson TJ, et al. (2009) Lutein accumulation in the absence of zeaxanthin restores nonphotochemical quenching in the arabidopsis thaliana npq1 mutant. Plant Cell 21:1798–1812.

Lindner M, Maroschek M, Netherer S et al. (2010) Climate change impacts, adaptive capacity, and vulnerability of European forest ecosystems. For Ecol Manage 259:698–709.

Martín-García J, Solla A, Corcobado T, Siasou E, Woodward S (2015) Influence of temperature on germination of *Quercus ilex* in *Phytophthora cinnamomi*, *P. gonapodyides*, *P. quercina* and *P. psychrophila* infested soils. For Pathol 45:215–223.

Martínez-Vilalta J, Lloret F, Breshears DD (2012) Drought-induced forest decline: causes, scope and implications. Biol Lett 8: 689–691.

Matesanz S, Valladares F (2014) Ecological and evolutionary responses of Mediterranean plants to global change. Environ Exp Bot 103:53–67.

Montserrat-Martí G, Camarero JJ, Palacio S, Pérez-Rontomé C, Milla R, Albuixech J, Maestro M (2009) Summer-drought constrains the phenology and growth of two coexisting Mediterranean oaks with contrasting leaf habit: Implications for their persistence and reproduction. Trees 23:787–799.

Moreno G, Pulido F (2009) The functioning, management and persistence of dehesas. In: Rigueiro-Rodríguez A, McAdam J, Mosquera-Losada MR (eds) Agrofor Eur., vol. 5. Kluwer, Dordrecht, The Netherlands, pp. 127–160.

Munné-Bosch S (2005) The role of α-tocopherol in plant stress tolerance. J Plant Physiol 162:743–748.

Munné-Bosch S, Alegre L (2000) Changes in carotenoids, tocopherols and diterpenes during drought and recovery, and the biological significance of chlorophyll loss in Rosmarinus officinalis plants. Planta 210:925–931.

Munné-Bosch S, Lalueza P (2007) Age-related changes in oxidative stress markers and abscisic acid levels in a drought-tolerant shrub, *Cistus clusii* grown under Mediterranean Weld conditions. Planta 225:1039–1049.

Nakagawa S, Johnson PCD, Schielzeth H (2017) The coefficient of determination R2 and intra-class correlation coefficient from generalized linear mixed-effects models revisited and expanded. J R Soc Interface 14:1–11.

Nakazawa M (2019) fmsb: Functions for medical statistics book with some demographic data. R Package version 070. https://cran.r-project.org/package=fmsb (18 June 2020, date last accessed).

Natalini F, Alejano R, Vázquez-Piqué J, Cañellas I (2016) The role of climate change in the widespread mortality of Holm oak in open woodlands of Southwestern Spain. Dendrochronologia 38: 51–60.

Niinemets Ü (2010) Responses of forest trees to single and multiple environmental stresses from seedlings to mature plants: Past stress history, stress interactions, tolerance and acclimation. For Ecol Manage 260:1623–1639.

Niinemets Ü, Lukjanova A (2003) Total foliar area and average leaf age may be more strongly associated with branching frequency than with leaf longevity in temperate conifers. New Phytol 158: 75–89.

Niinemets Ü, Cescatti A, Rodeghiero M, Tosens T (2005) Leaf internal diffusion conductance limits photosynthesis more strongly in older leaves of Mediterranean evergreen broad-leaved species. Plant Cell Environ 28:1552–1566.

Nogués I, Llusià J, Ogaya R, Munné-Bosch S, Sardans J, Peñuelas J, Loreto F (2014) Physiological and antioxidant responses of *Quercus ilex* to drought in two different seasons. Plant Biosyst 148: 268–278.

Ogaya R, Peñuelas J (2006) Contrasting foliar responses to drought in *Quercus ilex* and *Phillyrea latifolia*. Biol Plant 50:373–382.

Ogaya R, Liu D, Barbeta A, Peñuelas J (2020) Stem mortality and forest dieback in a 20-years experimental drought in a Mediterranean holm oak forest. Front For Glob Chang 2:89.

Peguero-Pina JJ, Morales F, Flexas J, Gil-Pelegrín E, Moya I (2008) Photochemistry, remotely sensed physiological reflectance index and de-epoxidation state of the xanthophyll cycle in *Quercus coccifera* under intense drought. Oecologia 156:1–11.

Pinheiro J, Bates D, DebRoy S, Sarkar D, Team RC (2020) nlme: Linear and nonlinear mixed effects models. R Package version 31-148. https://cran.r-project.org/package=nlme (27 May 2020, date last accessed).

Pollastrini M, Feducci M, Bonal D et al. (2016) Physiological significance of forest tree defoliation: Results from a survey in a mixed forest in Tuscany (central Italy). For Ecol Manage 361:170–178.

Pollastrini M, Puletti N, Selvi F, Iacopetti G, Bussotti F (2019) Widespread crown defoliation after a drought and heat wave in the forests of Tuscany (central Italy) and their recovery—A case study from summer 2017. Front For Glob Chang 2:74.

Poyatos R, Aguadé D, Galiano L, Mencuccini M, Martínez-Vilalta J (2013) Drought-induced defoliation and long periods of near-zero gas exchange play a key role in accentuating metabolic decline of Scots pine. New Phytol 200:388–401.

Pulido F, Díaz M, Sebastian J (2001) Size structure and regeneration of Spanish holm oak *Quercus ilex* forests and dehesas: effects of agroforestry use on their long-term sustainability. For Ecol Manage 146:1–13.

R Development Core Team (2020) R (v. 4.0.0, 2020): A language and environment for statistical computing. R Foundation for Statistical Computing, Vienna, Austria. http://www.r-project.org/ (24 September 2020, date last accessed).

Ramírez-Valiente JA, Koehler K, Cavender-Bares J (2015) Climatic origins predict variation in photoprotective leaf pigments in response to drought and low temperatures in live oaks (*Quercus* series *Virentes*). Tree Physiol 35:521–534.

Ramírez-Valiente A, Opez RL, Hipp AL, Aranda I (2020) Correlated evolution of morphology, gas exchange, growth rates and hydraulics as a response to precipitation and temperature regimes in oaks (*Quercus*). New Phytol 227:794–809.

Resco De Dios V, Fischer C, Colinas C (2007) Climate change effects on mediterranean forests and preventive measures. New For 33: 29–40.

Rivas-Martínez S (1987) Memoria del mapa de series de vegetación de España. Ministerio de Agricultura, Pesca y Alimentación, Icona, Madrid.

Rodríguez A, Durán J, Rey A, Boudouris I, Valladares F, Gallardo A, Yuste JC (2019) Interactive effects of forest die-off and drying-rewetting cycles on C and N mineralization. Geoderma 333:81–89.

Sánchez ME, Caetano P, Ferraz J, Trapero A (2002) *Phytophthora* disease of *Quercus ilex* in south-western Spain. For Pathol 32:5–18.

Solla A, García L, Pérez A, Cordero A, Cubera E, Moreno G (2009) Evaluating potassium phosphonate injections for the control of *Quercus ilex* decline in SW Spain: Implications of low soil contamination by *Phytophthora cinnamomi* and low soil water content on the effectiveness of treatments. Phytoparasitica 37:303–316.

Stirbet A, Govindjee (2011) On the relation between the Kautsky effect (chlorophyll a fluorescence induction) and Photosystem II: Basics and applications of the OJIP fluorescence transient. J Photochem Photobiol B Biol 104:236–257.

Strasser RJ, Srivastava A, Tsimilli-Michael M (2000) The fluorescence transient as a tool to characterize and screen photosynthetic samples. Probing Photosynth Mech Regul Adapt 443–480.

Tausz M, Wonisch A, Grill D, Morales D, Soledad Jiménez M (2003) Measuring antioxidants in tree species in the natural environment: From sampling to data evaluation. J Exp Bot 54:1505–1510.

Tausz M, Šircelj H, Grill D (2004) The glutathione system as a stress marker in plant ecophysiology: Is a stress-response concept valid? J Exp Bot. 55:1955–1962.

Thomas FM (2008) Recent advances in cause-effect research on oak decline in Europe. CAB Reviews: Perspectives in Agriculture, Veterinary Science, Nutrition and Natural Resources 2008. 3: No. 037, pp 1–12.

Toms J, Lesperance M (2003) Piecewise regression: A tool for identifying ecological thresholds I. Ecology 84:2034–2041.

Valladares F, Martinez-Ferri E, Balaguer L, Perez-Corona E, Manrique E (2000) Low leaf-level response to light and nutrients in Mediterranean evergreen oaks: A conservative resource-use strategy? New Phytol 148:79–91.

Vidi PA, Kanwischer M, Baginsky S, Austin JR, Csucs G, Dörmann P, Kessler F, Bréhélin C (2006) Tocopherol cyclase (VTE1) localization and vitamin E accumulation in chloroplast plastoglobule lipoprotein particles. J Biol Chem 281:11225–11234.

Vito MRM (2008) Segmented: an R package to fit regression models with broken-line relationships. R News 8:20–25.

Vranova E, Inze D, Van Breusegem F (2002) Signal transduction during oxidative stress. J Exp Bot 53:1227–1236.

Xiong Y, D'Atri JJ, Fu S, Xia H, Seastedt TR (2011) Rapid soil organic matter loss from forest dieback in a subalpine coniferous ecosystem. Soil Biol Biochem 43:2450–2456.

Zarco-Tejada PJ, Camino C, Beck PSA et al. (2018) Previsual symptoms of *Xylella fastidiosa* infection revealed in spectral plant-trait alterations. Nat Plants 4:432–439.

Zarter CR, Adams WW, Ebbert V, Cuthbertson DJ, Adamska I, Demmig-Adams B (2006) Winter down-regulation of intrinsic photosynthetic capacity coupled with up-regulation of Elip-like proteins and persistent energy dissipation in a subalpine forest. New Phytol 172: 272–282.